SAND2014-15525C

Direct Observation of Grain Boundary PN Junction Potentials in CIGS Using Photoemission and Low Energy Electron Microscopy (PELEEM)

Calvin K. Chan[1*], Taisuke Ohta[1,2], Gary L. Kellogg[1,2],
Lorelle Mansfield[3], Kannan Ramanathan[3], Rommel Noufi[3]

[1]Sandia National Laboratories, Albuquerque, NM 87185, United States
[2]Center for Integrated Nanotechnologies, Albuquerque, NM 87185, United States
[3]National Renewable Energy Laboratory, Golden, CO 80401, United States

***Abstract*— Spectroscopic microscopies with chemical and electronic structure information have become important tools for understanding the complex structure-property-performance relationships of high performing $Cu(In_{1-x}Ga_x)Se_2$ (CIGS) photovoltaic materials and devices. Here, we describe the application of spectrally resolved photoemission and low-energy electron microscopy (spec-PELEEM) to CIGS. With the ability to map relative electric potentials with high fidelity, a large variation in the built-in pn junction potential was observed at CIGS grain boundaries. In any given 20 μm region, the built-in voltage spanned the range from depletion (0.1 V) to inversion (1.4 V). These grain-to-grain variations could explain the electron collection efficiency of CIGS grain boundaries and devices. These results highlight the potential of spec-PELEEM to solve critical structure-property-performance issues facing compound thin-film materials.**

***Index Terms*—electron microscopy, photoelectron microscopy, photovoltaic cells, p-n junctions, spectroscopy, thin-film devices, II-VI semiconductor materials.**

I. Introduction

Copper indium gallium diselenide (CIGS) photovoltaic cells have demonstrated power conversion efficiencies of 20%, which are competitive with multicrystalline solar cells [1]. Despite this accomplishment, further advancement and manufacturing of CIGS photovoltaics has been limited by our understanding of fundamental materials problems such as phase segregation, junction and contact formation, and materials degradation. Meso and nanoscale variations in chemical composition cause local electronic structure inhomogeneities that greatly impact charge separation, charge transport, and carrier recombination. Understanding and controlling these properties has been limited by a lack of microscopy techniques with simultaneous spatial, chemical, electronic, and temporal sensitivity.

In the case of high-performance CIGS cells fabricated by a three-step physical vapor co-deposition process (PVD-CIGS) [2], the results of mesoscale diffusion have been observed in some microscopy studies. Variations in chemical composition [3]–[5], electronic structure [4], [6]–[10], and charge transport [11] have been observed at grain boundaries of PVD-CIGS. The high power conversion efficiencies of PVD-CIGS devices have been attributed to mesoscale Cu diffusion, where Cu deficiency at the grain boundaries form n-p homojunctions with the grain interior to suppress carrier recombination and enhance electron-hole separation. However, this simple picture is not sufficient to explain the performance of CIGS photovoltaic materials and devices. First, all the literature reports indicate a maximum of $\approx$ 0.5 V built-in potential, which is consistent with hole depletion, but not consistent with a fully inverted n-type region at the grain boundaries. This could be an artifact related to the surface sensitivity of the aforementioned techniques employed thus far, which only measure attenuated changes in a relatively homogeneous skin layer. An alternative theory is that the grain-to-boundary junction is only completed with the addition of CdS. Moreover, CIGS phase diagrams do not support a gradual nonstoichiometric transition from a Cu-poor "β-phase" to the $Cu(In,Ga)Se_2$ "α-phase" [12], [13]. Instead, a mixed α+β phase consisting of nanoscale phase segregated α and β domains is expected. This α+β region would occur between the grain boundary and the grain interior, and would effectively extend the length of the p-n junction. Given these questions surrounding the grain-to-boundary p-n junction in CIGS, a spectroscopic microscope with nanoscale resolution, chemical and electronic structure sensitivity, and real-time imaging is needed.

Here, we discuss our recent efforts to apply spectroscopic photoemission and low energy electron microscopy (spec-PELEEM) to better understand the chemical and electronic properties of CIGS photovoltaic materials. Based on low-energy electron microscopy (LEEM) [14], which is often used to study real-time film growth processes, our approach with spec-PELEEM collects spectrally resolved chemical and electronic structure information with nanometer spatial resolution. This technique effectively enables electron and photoemission spectroscopies with high fidelity spatial resolution.

II. Experimental Details

To benchmark the capabilities of our spec-PELEEM technique, high-performance PVD-CIGS materials were studied. A 3 in x 3 in PVD-CIGS sample (C3405) was fabricated using a 3-stage process in the CIGS Cluster Tool at the National Renewable Energy Laboratory (NREL) [2]. The sample consisted of 2 μm CIGS/0.6 μm Mo/2.5 mm soda lime glass. To enable top surface plan view imaging by LEEM and spec-PEEM, no additional top contact layers were deposited. X-ray fluorescence (XRF) was measured at the center of the

*Corresponding Author: cchan@sandia.gov

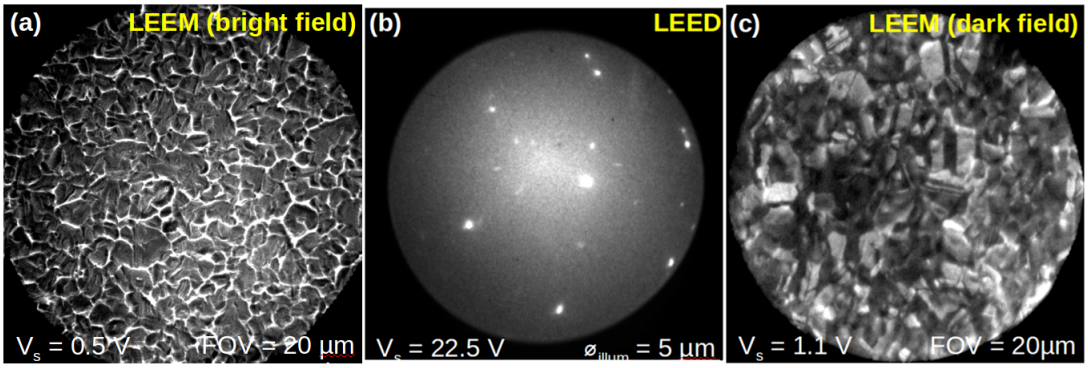

Fig. 1. (a) Bright-field LEEM image of PVD-CIGS at $V_s = 0.5$ V with a 20 μm field of view (FOV). (b) Selective area LEED diffraction pattern using a 5 μm aperture over a large grain. (c) Dark-field LEEM image using a diffraction aperture to filter out the secondary electrons.

sample, showing Cu(III) and Ga(III) ratios of 0.913 and 0.39, respectively. These values are consistent with the literature for a high efficiency Cu($In_{0.7}$Ga_0.3)Se_2 device with 1.2 eV bandgap and 20% efficiency. The samples were packaged in dry nitrogen and sent to Sandia National Laboratories in Albuquerque, NM (SNL), where they were stored in a continuously purged nitrogen box. The PVD-CIGS sample was removed from nitrogen, cleaved into *approx* 1 cm x 1 cm subsamples, mounted onto a spec-PELEEM sample cartridge, and transferred into the spec-PELEEM ultrahigh vacuum system without further preprocessing. Prior to imaging, the samples were heated to 300 °C for several hours to remove water and hydrocarbon contamination on the surface. Previous studies showed that CIGS films deposited at high temperatures do not undergo any significant structural changes with post-deposiiton annealing [15].

Spec-PELEEM measurements were conducted using an Elmitec GmbH LEEM III system equipped with a hemispherical imaging energy analyzer. A field emission electron source was used for low-energy electron imaging; a broadband Hg arc lamp with UV emission between 3.40-4.88 eV was used for general purpose non-spectroscopic photoemission imaging; and a VG Scienta VUV5000 He rf-plasma discharge lamp was used for spectroscopic PEEM. The plasma discharge lamp provided sharper and higher energy primary lines at 21.22 eV (He I) and 40.8 eV (He II) for higher fidelity spec-PEEM measurements. An important variable in the spec-PELEEM measurement is the start voltage V_s, which is the potential bias between the electron gun and the sample. In (spec-)LEEM, V_s is equal to the kinetic energy of incoming and outgoing electrons with an offset for the local work function. In spec-PEEM, V_s reperesents the relative energy window offset that is being observed by the electron energy analyzer.

III. Results & Discussion

Non-spectroscopic PEEM was first performed on a coupon from the three-stage PVD Cu($In_{0.7}$Ga_0.3)Se_2 sample (C3405). As loaded, the sample exhibited high average pixel intensities > 500 counts when illuminated with the Hg lamp. However, no PEEM intensity was observed with the Hg lamp once the sample was heated to 300 300 °C for several hours. Since photoemission only occurs when the photoexcitation energy (3.4-4.9 eV) is greater than the work function of the sample surface, these observations are consistent with the work function of typical hydrocarbon contaminated surfaces (4.2-4.6 eV) and clean CIGS surfaces (5.3-5.4 eV).

Figure 1(a) shows a representative bright-field LEEM image (FOV = 20 μm, $V_s = 0.5$ V) of a PVD-CIGS sample. At these imaging conditions with low V_s, secondary electron emission from lower work function areas such as the CIGS grain boundaries dominate. These micrographs are remarkably similar to grain boundary images obtained using scanning Kelvin probe microscopy of similar samples [10]. This further confirms other work showing lower work functions at CIGS grain boundaries [4], [6]–[9].

Using a 5 μm illumination (area selective) aperture and rastering the sample position, LEED patterns were observed across the PVD-CIGS surface. Across most areas of the sample, multiple diffuse hexagonal diffraction patterns were observed, many of which translated laterally with changes in the electron kinetic energy ($\sim V_s$). These LEED behaviors indicate a microcrystalline and faceted grain structure with average grain sizes < 5 μm. In some locations with larger grains, a single bright LEED pattern was observed (Figure 1(b)). The hexagonal diffraction pattern is consistent with the reciprocal space features of the 112 surface plane of CIS [16], which is indeed faceted with respect to the CIGS (220)/(204) preferred growth direction [17]. The diffuse diffraction background was attributed to electron scattering, where the diffraction background is even more intense at lower V_s due to secondary electron emission. Using a diffraction aperture, dark-field LEEM imaging was conducted by blocking out these background contributions at low V_s. This filters out the high intensity, low work function CIGS grain boundary highlights. As shown in Figure 1(c), this enables the imaging of the finer grain details.

To obtain a quantitative measure of the changes in local work function when going from grain interior to grain boundary in CIGS, spectroscopic imaging was obtained by taking consecutive dark-field LEEM images (FOV = 20 μm)

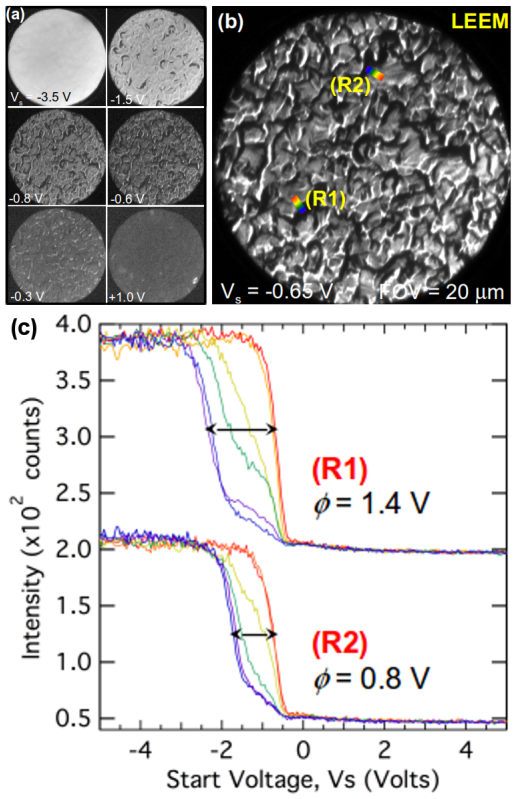

Fig. 2. LEEM-IV on PVD-CIGS. (a) LEEM images (FOV = 20 μm) were taken with V_s from -5 V to $+5$ V in 0.1 V increments. (b) A single LEEM image at $V_s = -0.65$ V from the LEEM-IV scan showing two representative regions, R1 and R2. (c) The intensity vs. V_s spectra along the two different line scans across grain boundaries, R1 and R2, shown in the LEEM image.

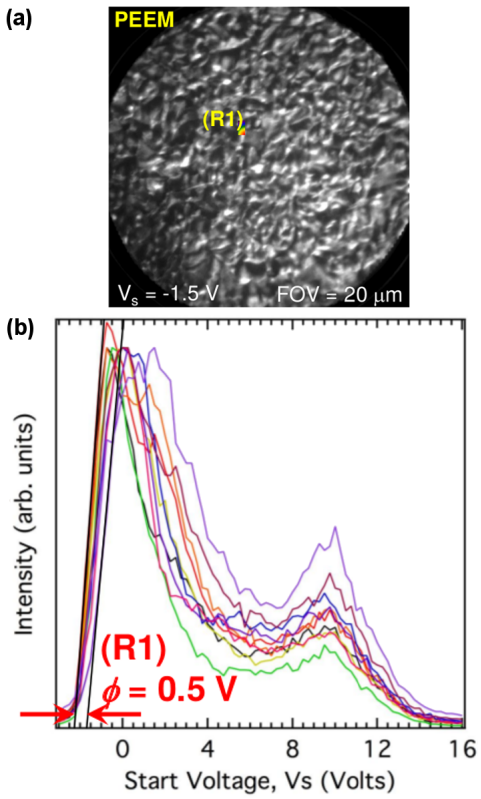

Fig. 3. PEEM-IV on PVD-CIGS. PEEM images (FOV = 20 μm) were taken with V_s varied from -3 V to $+17$ V in 0.2 V increments. (a) A single 20 μm $\times$ 20 μm PEEM image at V_s = -1.5 V from the PEEM-IV scan. (b) The intensity vs. V_s spectra along the line scan across a CIGS grain boundary shown in R1 of the PEEM image.

while sweeping the electron kinetic energy (-5.0 V $\geq V_s \leq$ +5.0 V) in 50 meV increments. Figure 2(a) shows a small selection of LEEM images at various V_s to highlight changes in intensity with electron energy. A micrograph at $V_s = -0.65$ V of the examined region is shown in Figure 2(b). For every pixel in the image, an intensity vs. V_s (IV) spectrum was collected. As two examples, the IV for 12 spots along the R1 and R2 line scans (resolution 50-100 nm) in the LEEM image is plotted in Figure 2(c). In these LEEM-IV spectra, the intensity onset represents the local work function. At V_s below this cutoff, electrons have less energy than the work function and are reflected from the sample, resutling in higher LEEM intensities. At voltages above this cutoff, electrons have high enough energies to be captured by the sample, resulting in lower intensities. Therefore, changes in the LEEM-IV onset represent changes in local work function (band bending or built-in voltage). In R1, the potential variation from the grain interior to the grain boundary is -1.4 V. In R2, this built-in potential is -0.8 V. Manually inspecting over the entire image, CIGS built-in potentials between the grain interior and respective grain boundaries (ϕ) varied significantly between -0.5 to -1.4 V. This significant variation suggests that CIGS grain-to-grain junctions may vary from depleted to inverted depending on location, which is one possible reason for inconsistent CIGS device performance and reproducibility. Previous reports have also shown similar grain-to-grain variations in the electron collection efficiency, built-in voltage, and n-type inversion at CIGS grain boundaries. But, the magnitude of the built-in voltages measured here are larger than those reported in the literature ($\sim$ 0.5 V or less). We believe that the values measured here using LEEM is more reflective of the junction built-in potential because low energy electrons carry more information depth than scanning probes and higher energy scanning electron techniques.

To access the valence band of CIGS, spec-PEEM was conducted similarly to LEEM-IV. While no PEEM intensity was observed using the Hg arc lamp ($h\nu_{\mathrm{Hg}} < \Phi_{\mathrm{CIGS}}$), the higher photon energies of the He rf-plasma discharge lamp provided ample photoemission intensities to perform PEEM measurements. PEEM-IV was performed by taking sequential PEEM images (FOV = 20 m) of the PVD-CIGS sample as V_s was varied from -3 V to $+17$ V in 0.2 V increments. A representative PEEM image at $V_s = -1.5$ V is shown in Figure 3a. The PEEM-IV spectrum for 10 points along the R1 line scan shown in Figure 3a – across a representative CIGS grain boundary – is plotted in Figure 3b. Each line in Figure 3b is effectively an ultraviolet photoemission spectrum (UPS) with a spatial resolution of $\sim$ 50-100 nm. In a PEEM-

IV spectrum, The local work function is determined by the secondary electron cutoff (SEC), which is observed as the onset of photoemission below $V_s = 0$ V here. Across the R1 grain boundary a relative change in the work function by -0.5 eV was observed when going from the CIGS grain interior to the grain boundary. Manual inspection over the entire FOV revealed grain boundary potentials that varied from 0.0 eV to -0.5 eV. These values are much lower than what was previously observed with LEEM-IV, but are more consistent with values obtained from SEC measurements using a scanning electron microscope (SEM) [4], work function measurements from scanning Kelvin probe microscopy (SKPM) [10], and scanning tunneling microscopy/spectroscopy (STM/STS) [9].

Furthermore, the valence states observed in PEEM-IV spectra between $V_s = 6$ V and 16 V show a commensurate shift towards higher binding energies (lower V_s) by -0.5 eV when going from the grain interior to the grain boundary. This rigid shift of the work function and the valence states confirm an electrostatic built-in field near CIGS grain boundaries. Since the Fermi level (E_F) is not visible in the spectra, and was not previously referenced for prior to this measurement, the absolute binding energy values of the valence states could not be determined. However, the position of the Fermi level can be estimated from the measured SEC and assuming a work function of clean CIGS:

$$\Phi = E_o + h\nu - E_F$$

where $\Phi \sim 5.3$ eV is the CIGS work function, E_o is the secondary electron cutoff, and $h\nu = 21.22$ eV is the photon energy of the He I excitation line. From this, the estimated E_F of the system is 13.9 eV, and the broad valence feature observed in Figure 3b is determined to sit between -6 eV and -1 eV binding energy with respect to E_F. The spectra compare very well to area-integrated He I photoemission data available for CIGS in the literature [5]. Comparing to similar area-integrated He II photoemission data [17], [18], the valence band features observed here are likely a superposition of Cu 3d, Se 4p, and Group III-oxides. The differences between He I and He II spectra are due to $h\nu$-dependent photoemission cross-sections. Despite the availability of He II irradiation in our He rf-plasma discharge lamp, we were unable to obtain He II PEEM-IV data for direct comparison with the literature data because of its very low intensity. Nevertheless, an important conclusion from these PEEM-IV measurements is the presence of significant oxide components on the sample. This was expected since these samples were cleaned only with thermal annealing in vacuum, and not with NH_3 or ion sputtering prior to imaging.

This discrepancy in the built-in voltage as measured by PEEM-IV and LEEM-IV can be attributed to differences in the probing depth of the techniques. Analogous to conventional area-integrated photoemission spectroscopy, PEEM-IV measures work functions determined by the sample surface and collects photoexcited valence electrons coming from 2-5 nm below the surface. These probing depths are similar to those examined using scanning probe and SEM techniques. Since these techniques probe only the skin layer of the CIGS grains, they never fully capture the buried p-n junction interface. This results in the attenuated built-in voltages of 0.0-0.5 eV. In contrast, LEEM-IV collects low energy backscattered electrons or electrons that have interacted with the internal electrostatic field of the sample. As a result, LEEM-IV probes deeper into the sample (50-100 nm). This allows LEEM-IV to potentially capture the full 0.5-1.4 eV built-in potential established by the p-n junction between the grain interior and the grain boundary.

IV. Summary

Spectroscopic microscopies with chemical and electronic structure information have become important tools for understanding the complex structure-property-performance relationships of CIGS materials and devices. We applied spectrally resolved photoemission and low-energy electron microscopy (spec-PELEEM) techniques to PVD-CIGS grown by a 3-stage process at NREL. Consistent with the literature, these CIGS films exhibited microcrystalline morphologies with an average grain size of $\sim$ 1-5 μm, with a faceted $\{112\}$ surface termination. In LEEM, a large variation in the built-in potential ranging from -0.5 V to -1.4 V was observed when going from the grain interior to the grain boundary. A lower built-in potential up to -0.5 V was observed using PEEM. The discrepency can be explained by the different information depth between low-energy backscattered electrons and photoemission electrons. We believe that the higher built-in potentials measured using LEEM are a more accurate reflection of the full built-in voltage of the buried CIGS pn junction. The large grain-to-grain fluctuations in this built-in potential may explain the challenges in reproducing and manufacturing CIGS devices, and may provide ultimate limitations on certain device parameters. These are the first reported results of spec-PELEEM being used to image potential variations in a technologically relevant photovoltaic material, which highlights the potential for such a tool to solve critical structure-property-performance issues facing compound thin-film materials.

Acknowledgments

The authors thank Dr. C.B. Diaconescu and G. Copeland for experimental assistance. This work was supported by a U.S. Department of Energy, Office of Energy Efficiency and Renewable Energy Sunshot Initiative award for Bridging Research Interactions through Collaborative Development Grants in Energy (BRIDGE, DE-FOA-0000654 CPS25859). Some work performed in collaboration with the Center for Integrated Nanotechnologies (CINT), an Office of Science User Facility operated for the U.S. Department of Energy Office of Science. T.O. also acknowledges support from the U.S. Department of Energy, Office of Science, Office of Basic Energy Sciences, Division of Materials Science and Engineering; and Sandia National Laboratories' Laboratory Directed Research and Development. Sandia National Laboratories is a multi-program laboratory managed and operated by Sandia Corporation, a wholly owned subsidiary of Lockheed Martin Corporation, for

the U.S. Department of Energy's National Nuclear Security Administration under contract DE-AC04-94AL85000.

REFERENCES

[1] P. Jackon, et al., "New world record efficiency for Cu(In,Ga)Se_2 thin-film solar cells beyond 20%," *Prog. Photovolt: Res. Appl.* vol. 19(894), pp. 894-897, 2011.

[2] I. Repins, et al., "19.9%-efficient ZnO/CdS/ CuInGaSe_2 Solar Cell with 81.2% Fill Factor," *Prog. Photovolt: Res. Appl.* Vol. 16, 235-239, 2009.

[3] D. Abou-Ras, et al., "Direct Insight into Grain Boundary Reconstruction in Polycrystalline Cu(In,Ga)Se_2 with Atomic Resolution," *Phys. Rev. Lett.* vol. 108, 075502. 2012.

[4] M.J. Hetzer, et al., "Direct observation of copper depletion and potential changes at copper indium gallium diselenide grain boundaries," *Appl. Phys. Lett.* vol. 86, 162105. 2005.

[5] D. Liao, et al., "Cu depletion at the CuInSe_2 Surface," *Appl. Phys. Lett* Vol. 82(17), pp2829-2831, 2003.

[6] S. Sadewasser, et al., "Kelvin probe force microscopy for the nanoscale characterization of chalcopyrite solar cell materials and devices" *Thin Solid Films* Vol. 431-432, pp257-261, 2003.

[7] G. Hanna, et al., "Texture and electronic activity of grain boundaries in CuIn,GaSe_2 thin films," *Appl. Phys. A - Mater. Sci. Proc.* Vol. 82, pp1-7, 2006.

[8] U. Rau, et al., "Grain boundaries in Cu(In,Ga)$(Se,S)_2$ thin-film solar cells," *Appl. Phys. A - Mater. Sci. Proc.* Vol. 96, pp221-234, 2009.

[9] D. Azulay, et al., "Microscopic evidence for the modification of the electronic structure at grain boundaries of Cu($In_{1-x}Ga_xSe_2$ films," *Phys. Rev. Lett.* Vol 108, p076603, 2012.

[10] C.-S. Jiang, et al., "Local built-in potential on grain boundary of Cu(In,Ga)Se_2" thin films, *Appl. Phys. Lett.* vol. 84, 3477, 2004.

[11] D. Azulay, et al., "Current routes in polycrystalline CuInSe_2 and Cu(In,Ga)Se_2 films," *Solar Energy Mater. Solar Cells* Vol 91(1), pp8590, 2007.

[12] B. Stanbery, "Copper indium selenides and related materials for photovoltaic devices," *Crit. Rev. in Sol. State Mater. Sci.* Vol 27(2), pp73117, 2002.

[13] R. Herberholz, et al., "Phase segregation, Cu migration and junction formation in Cu(In,Ga)Se_2," *Eur. Phys. J. - Appl. Phys.*, Vol. 6(02), pp131139, 1999.

[14] E Bauer, "Low energy electron microscopy.," *Rep. Prog. Phys.,* Vol. 57(9), pp895, 1994.

[15] J. Wilson, et al., "In-situ Post-deposition Thermal Annealing of Co-evaporated Cu(InGa)Se_2 Thin Films Deposited at Low Temperatures," *Proc. 34th IEEE Photovolt. Specialists Conf.*, Philadelphia, PA, June 8-12, 2009.

[16] M. Contrera, et al., "Texture manipulation of CuInSe_2 thin films," *Thin Solid Films*, Vol. 361, pp167-171, 2000.

[17] D. Liao, et al., "Epitaxial growth of Cu(In, Ga)Se_2 on GaAs(110)," *J. Appl. Phys.*, Vol. 91(4), 1434549, 2002.

[18] M. Bär, et al., "The heavily intermixed In_2S_3/Cu(In,Ga)Se_2 interface as revealed by photoelectron and soft x-ray emission spectroscopy," *Proc. 39th IEEE Photovolt. Spec. Conf.*, Vol. 771, 0624030816, 2013.